Appendix E: Cell Uptake Studies of 4G Targeting Polyamides

The research in this appendix is an extension of results from a combination of Chapter 7 and 8. Julie A. Poposki (Caltech) is thanked for HeLa cell culture work and assistance with cell uptake experiments.

Abstract

A benzimidazole-containing polyamide targeted to the sequence 5'-WGGGGW-3' was discovered to have fluorescent properties in aqueous solution in the presence and absence of DNA. This set of properties allowed for the unique opportunity to interrogate polyamide cell uptake in the absence of fluorophore conjugation, which alters the molecular architecture of a compound and often influences cell permeability. A 23-member library of the core benzimidazole polyamide with variations at the tail and turn was synthesized and uptake properties were evaluated in HeLa cells using 2-photon confocal laser scanning microscopy. Investigations of cellular localization using organelle specific dyes were also conducted along with the elucidation of an efflux mechanism for certain polyamides in the library.

E.1 Introduction

The core benzimidazole containing polyamide **2** from Chapter 6[1] (Figure E.1) was discovered to possess a unique set of photophysical properties where the emission maximum was found to be 475 nm and the excitation maximum was λ = 330 nm. Excitation in the range of 380–390 nm was used to minimize photobleaching while still producing a detectible amount of emission at 500 nm. This inherent fluorescent property allowed for the unique opportunity to study cellular localization of this polyamide architecture without attachment of a fluorophore, which can often influence the cellular uptake process.[2-4] A library of polyamides (Figure E.2) containing the fluorescent core was synthesized, where the functionality at the turn and tail was modified in an effort to alter the overall uptake properties. HeLa cells were used for all studies and the polyamides were imaged using two-photon confocal laser scanning microscopy. After assessing the cellular uptake properties of the library of polyamide tail and turn modifications a study was conducted to determine the location of the polyamides in cells (mitochondria, nuclei, vessicals, lysozomes, etc.). Additionally, a polyamide that was found to remain extracellular was investigated to discriminate between cellular impermeability versus efflux using the the racemic efflux pump inhibitor (±)-Verapamil (2-(3,4-dimethoxyphenyl)-5-[2-(3,4-dimethoxyphenyl)ethyl-methyl-amino]-2-(1-methylethyl) pentanenitrile, CAS 52-53-9). The effect of ethanol fixing on the cellular uptake of polyamides as a function of time was also investigated and the ability of common transfection reagents to influence polyamide uptake was studied.

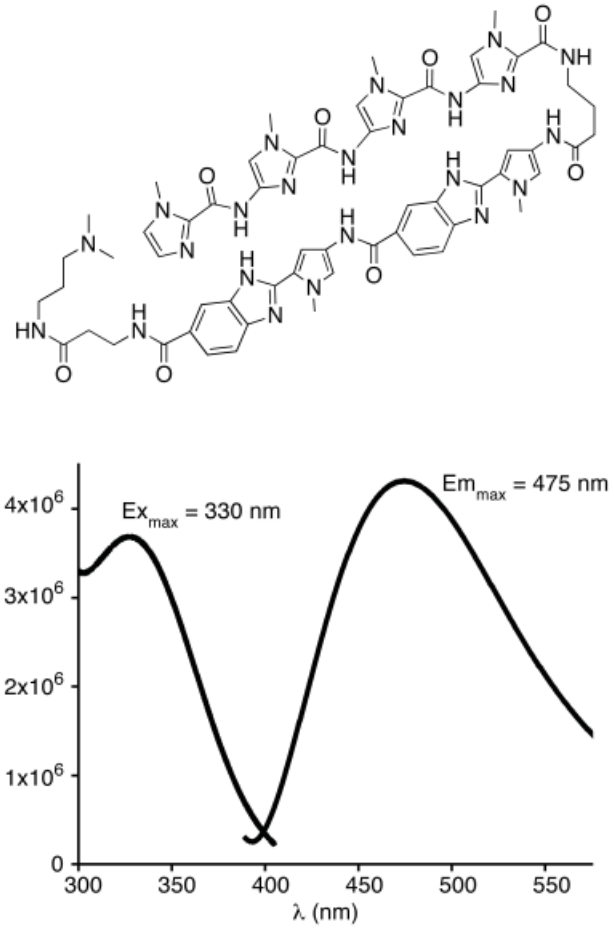

Figure E.1 Fluorescent polyamide **2** from Chapter 7 of this thesis. (bottom) Overlaid emission and excitation spectra of polyamide **2**.

E.2 Results and Discussion

A focused library of 23 compounds was synthesized containing tail and turn modifications on a common polyamide core (Figure E.2). The polyamide was synthesized on Kaiser Oxime resin by standard solid-phase synthesis methods as shown in Scheme E.1 to provide a base resin loaded with the desired polyamide core used for tail and turn diversification. With the core in hand, diversification commenced with deprotection and cleavage from resin to afford triamine derivatives **3**, **9**, **20**, **22**, and **23** (Scheme E.2). Deprotection and resin cleavage with a small set of amine nucleophiles produced compounds **1**, **2**, **4**-**8**, **10**, **11**, **13**-**16**, and **19**. Acylation prior to deprotection followed by cleavage from resin with amine nucleophiles produced compounds **12**, **17**, and **18**. Deprotection and cleavage from resin with lithium hydroxide produce compound **21**.

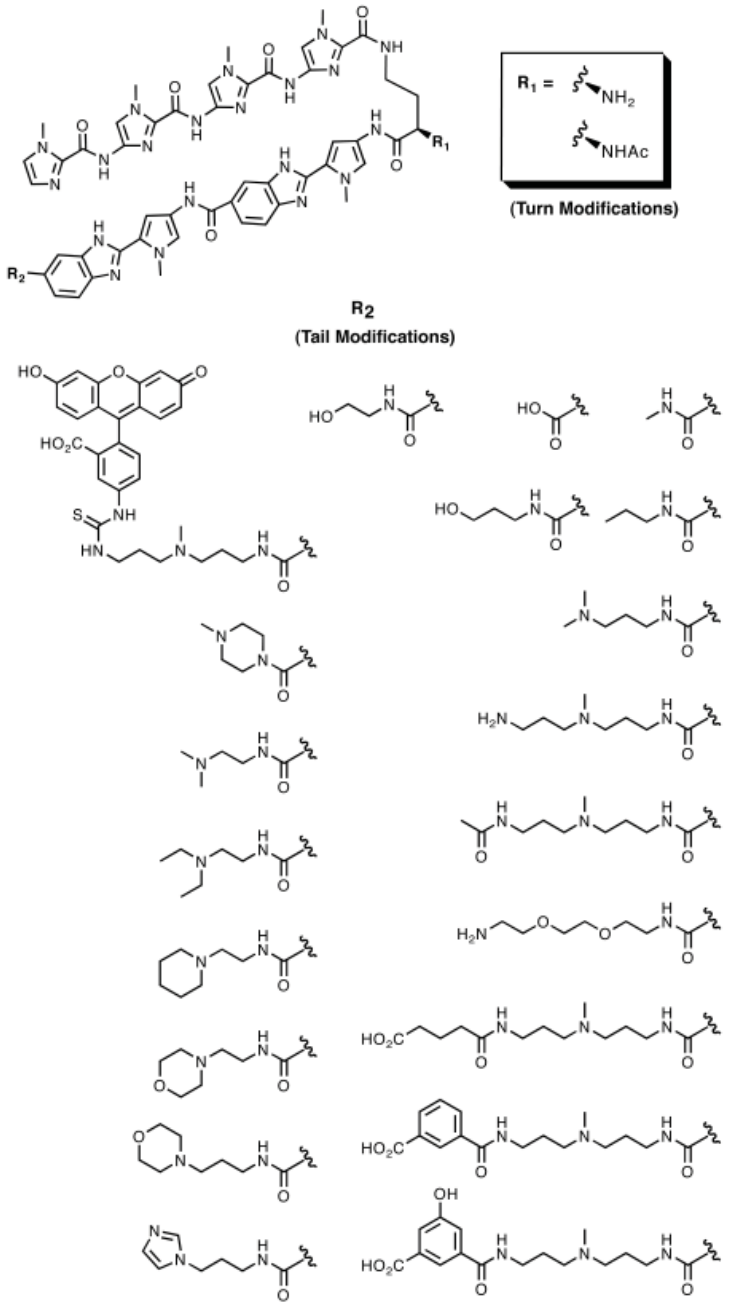

Figure E.2 Tail and turn modifications used for the contruction of a 23 compound benzimidazole-containing polyamide library.

The cell permeability of this small focused library of compounds was evaluated in HeLa cells using 2-photon laser-scanning confocal microscopy and the results are shown in Figures E.3–E.8. The results are grouped according to their cellular localization profile with Figures E.3–E.6 showing compounds that appear to be cell permeable but non-nuclear,

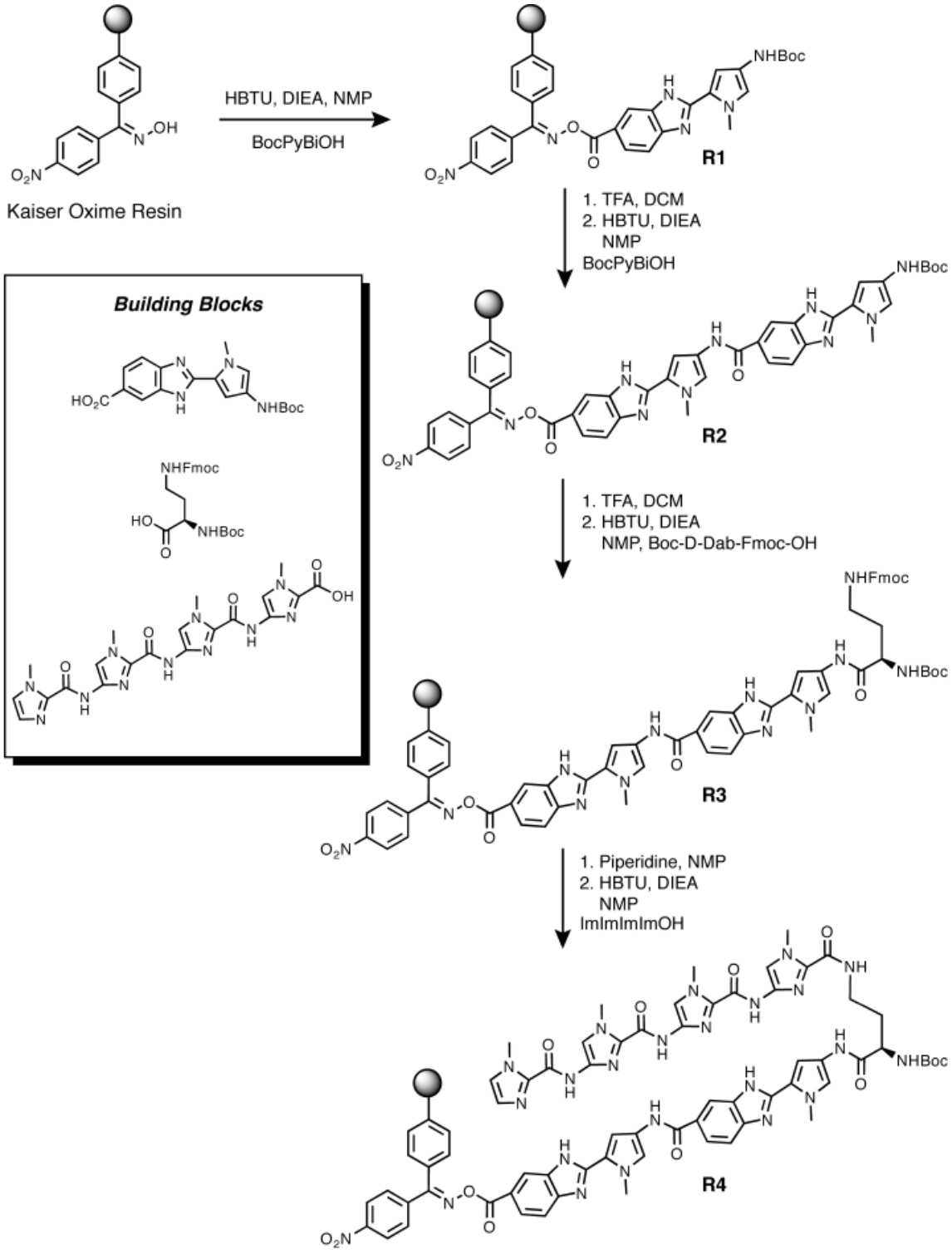

Scheme E.1. Synthesis of **R4**. Standard solid-phase synthesis methods from Chapter 7[1] were used.

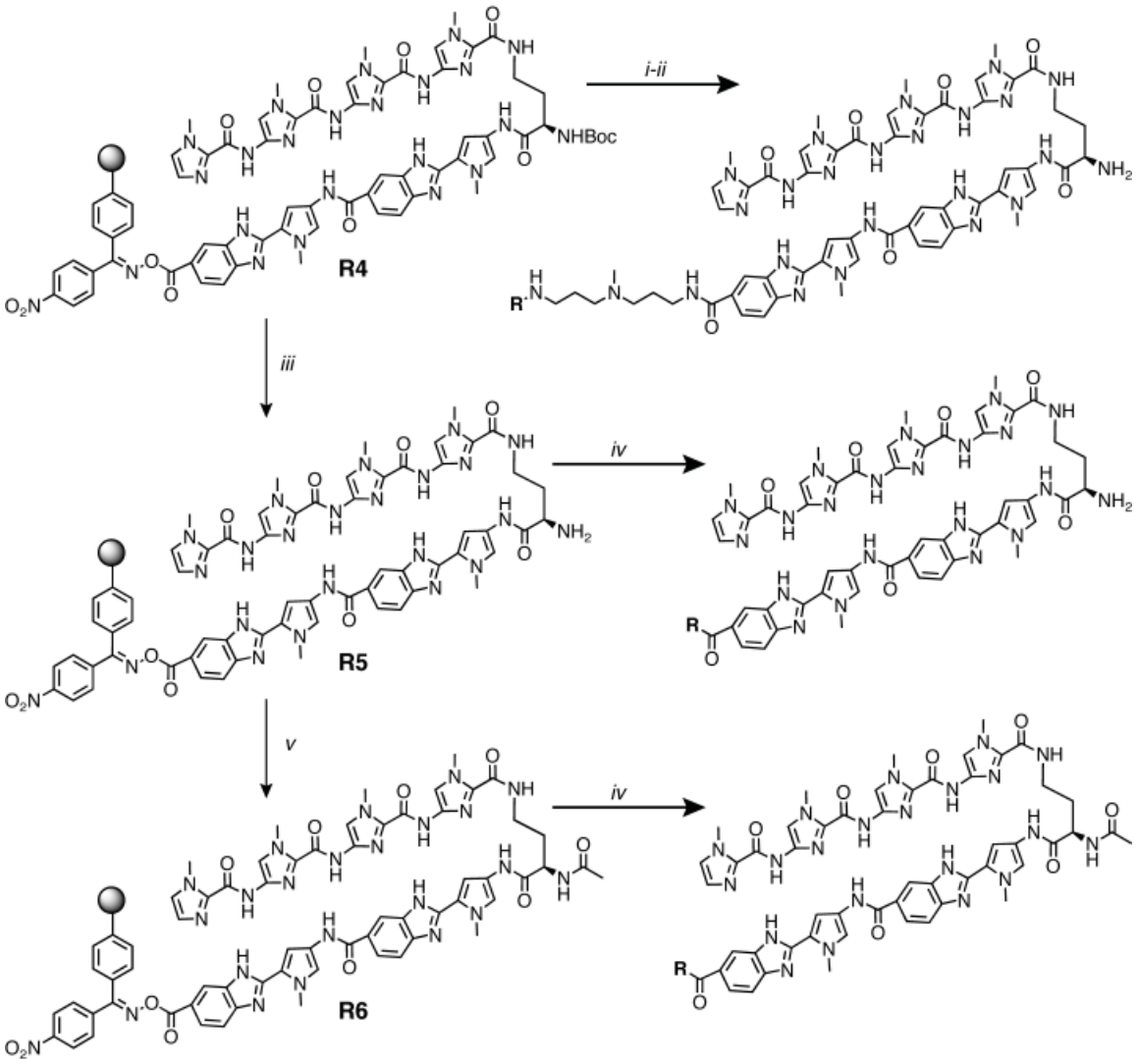

Scheme E.2. Synthesis of compound library. Reaction conditions: (*i)* NMP, Triamine, 80 ºC (Heat Block), 15-20 min; (*ii)* Conjugation to triamine, TFA, DCM; (*iii)* TFA, DMC; (*iv)* NMP, Nucleophile, 80 ºC (Heat Block), 15-20 min; (*v)* Ac_2O, NMP.

producing punctate cytoplastmic staining pattern. The compounds shown in Figure E.7 appear to be primarily extracellular and aggregated or precipitated with the first two compounds coating the exterior cell membranes. Figure E.8 shows compounds that are primarily extracellular although in a few cases there is a small amount of non-nuclear cellular localization observed.

In an effort to determine the location of the compounds inside the cells in Figures E.3–E.6 (punctate cytoplasmic staining) two organelle specific dyes were utilized. MitoTracker Red (CM-H2XRos) was used to asses the possibility of mitochondrial localization and LysoTracker Red (DND-99, a lysosome and trans-golgi stain) to asses localization in acidic lysosomes within the cell. Previous reports by Lown and coworkers demonstrated that a distamycin-fluorophore conjugate

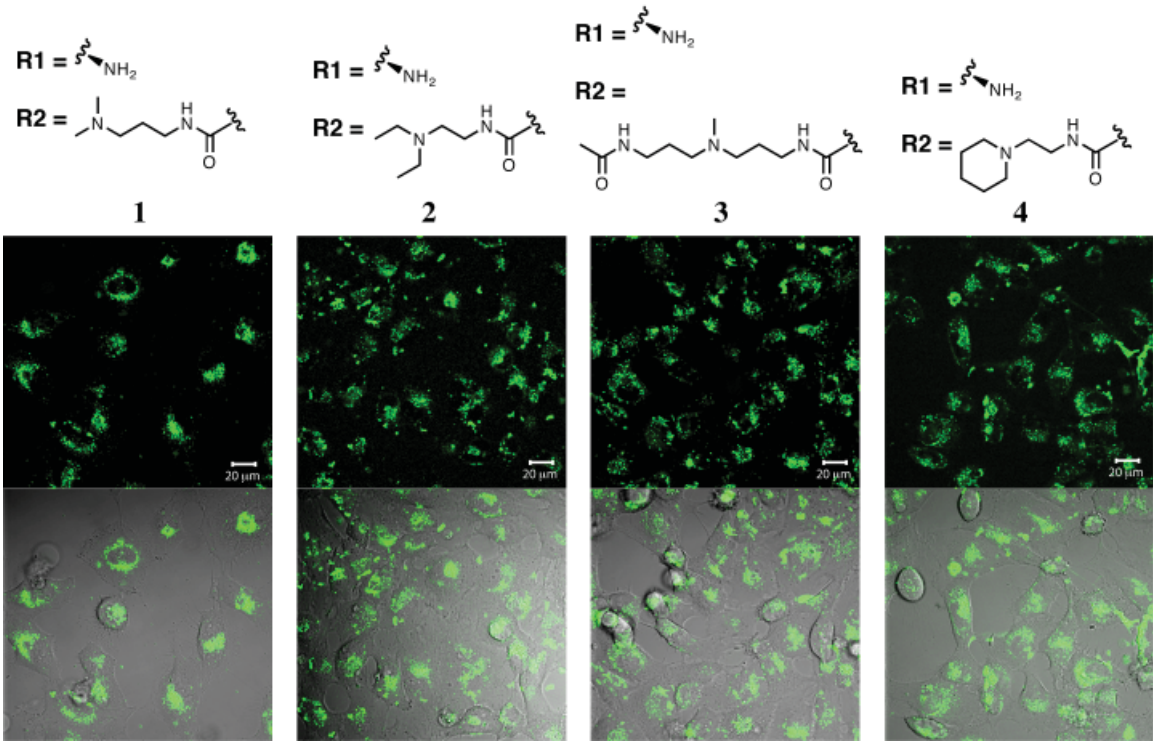

Figure E.3 Fluorescent polyamide cell uptake studies for compounds **1**-**4**. 2-Photon Laser Imaging Setup: Coherent Chameleon 2-photon Laser, (λ = 810 nm, 5% power), HFT KP 680 dichroic, BP 480-520 nm HeLa cells treated with 2mM **1**-**4** and imaged using 2-photon laser microscopy:

primarily localizes in the mitochondria of human ovarian adenocarcinoma cells.[5] The mechanism of mitochondrial staining by MitoTracker relies upon passive diffusion of the pro-fluorescent dye into the cell where it is oxidized and sequestered in the mitochondria (Figure E.9). Once in the mitochondria, nucleophilic attack resulting in thiol conjugation by proteins and peptides serves to retain the dye. Polyamide treated HeLa cells were dosed with MitoTracker prior to dual imaging using confocal laser scanning microscopy. The results show that the mitochondria appear as a diffuse cytoplasmic stain (Figure E.10, upper left live cell panel, magenta). The upper right panel shows the polyamide imaged with an orthogonal wavelength to Mitotracker and the bottom right panel shows that the two do not colocalize. It appears that the polyamide is not localized in mitochondria. Interestingly, ethanol fixing (fixed cell panel, bottom right, Figure E.10) of the cells leads to rapid nuclear trafficking of the polyamide however the diffuse mitochondria staining appears unchanged. It appears that unlike the Distamycin conjugates studied by Lown this class of polyamides does not localize in the mitochondria. However, this is not a surprising result given the dramatic differences in molecular structure and cell type.

Next, LysoTracker was used to determine if the polyamides were localized in acidic lysosomes of the cells. Figure E.11 shows the results of this study and it appears that the fluorescence

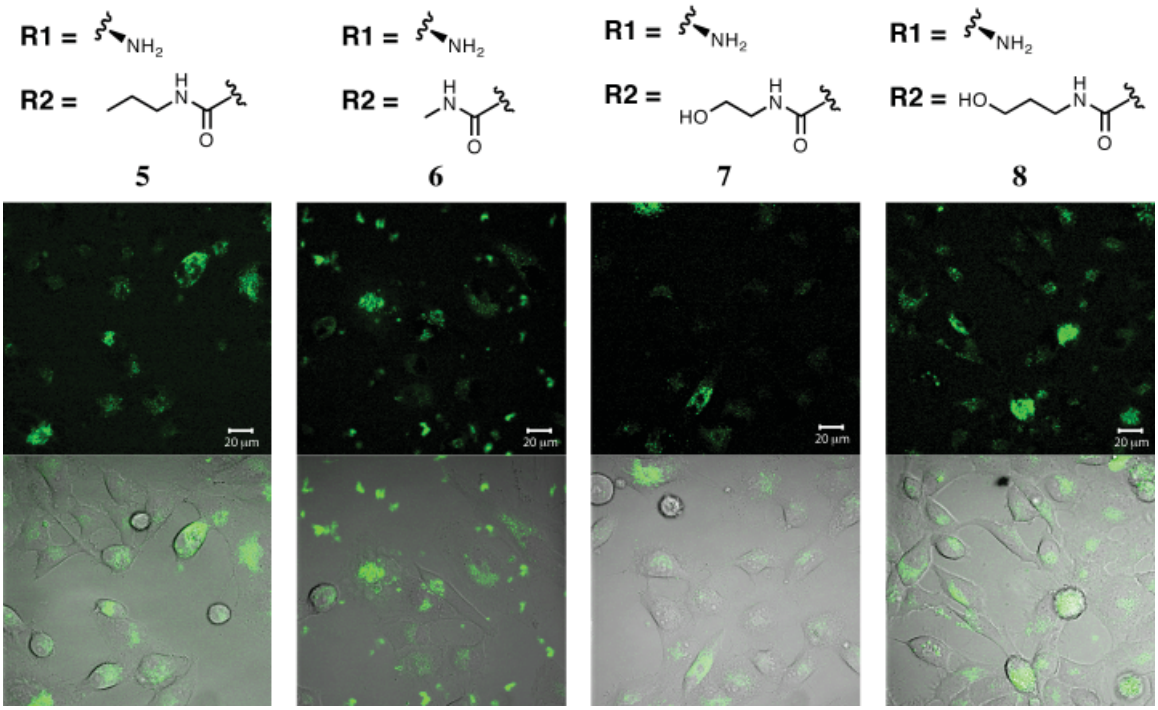

Figure E.4 Fluorescent polyamide cell uptake studies **5**-**8**. 2-Photon laser imaging setup and polyamide dosing concentration as described in Figure E.2.

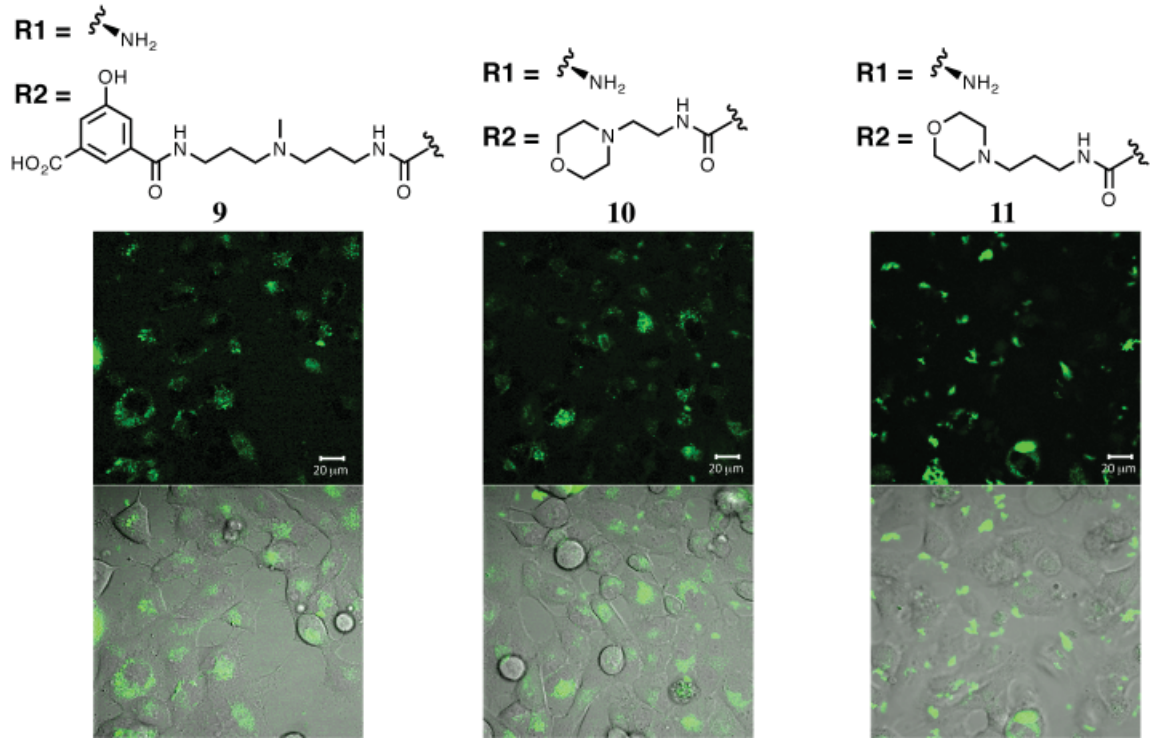

Figure E.5 Fluorescent polyamide cell uptake studies **9**-**11**. 2-Photon laser imaging setup and polyamide dosing concentration as described in Figure E.2.

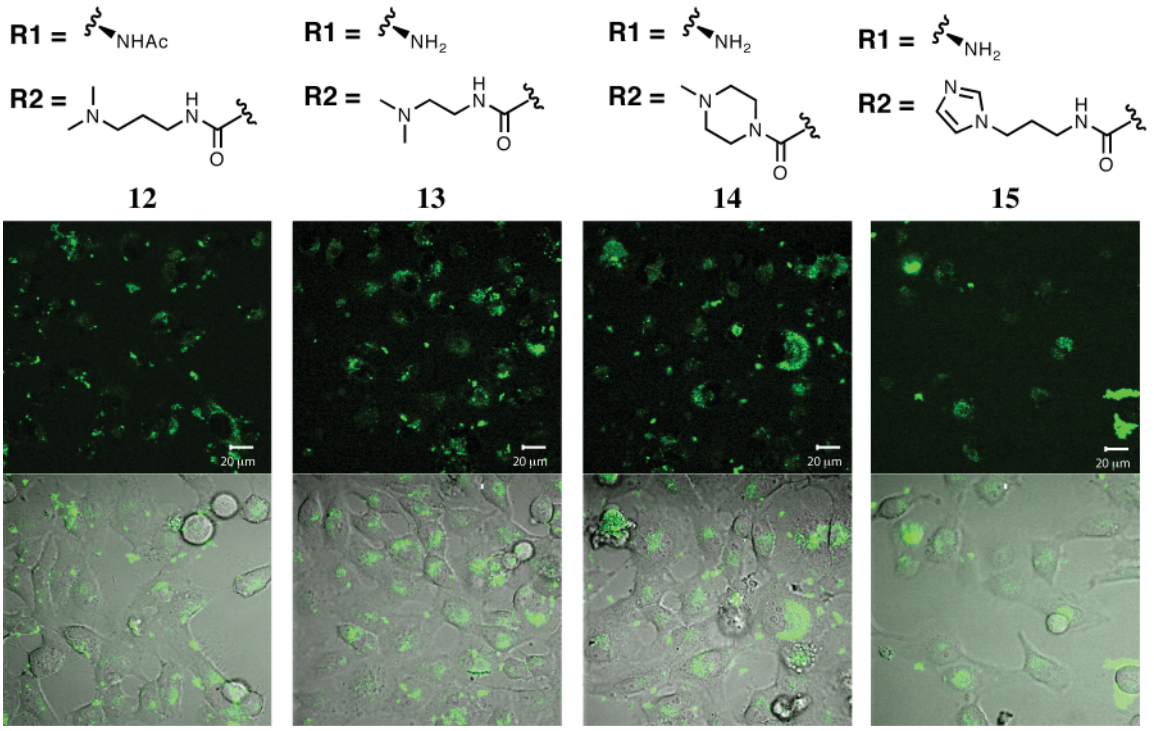

Figure E.6 Fluorescent polyamide cell uptake studies **12**-**15**. 2-Photon laser imaging setup and polyamide dosing concentration as described in Figure E.2.

signal of the internalized polyamides colocalizes with the fluorescence signal of LysoTracker, indicating that the polyamides are likely sequestered in acidic vessicles within the cells. This result is consistent with previous studies showing that in all cases 8-ring polyamides with 4 imidazoles show poor nuclear uptake profiles.[3] Weakly basic amines have also been shown to selectively accumulate within low pH cellular compartments such as lysosomes.[6] It should also be noted that the *N*,*N*-dimethylaminopropylamine tail commonly used to terminate polyamides and other classes of minor groove binders is very similar to the functionality present in LysoTracker responsible for targeting it to the lysosomes and acidic vessicles of cells. Additionally, high imidazole content has been correlated with low cell uptake and the four contiguous imidazoles in the polyamide core may be basic enough to target the polyamides to the lysosomes without the influence of any other functionality, however benzimidazole involvement can not be ruled out.[3,4]

The uptake properties of polyamide **23** in Figure E.8 were investigated in an effort to determine their mechanism of exclusion from the cells. Polyamide **23** (Figure E.8) dosed HeLa cells were treated with (±)-Verapamil and imaged using 2-photon laser confocal microscopy. The results in Figure E.12 show that treatment of polyamide dosed cells with (±)-Verapamil causes uptake

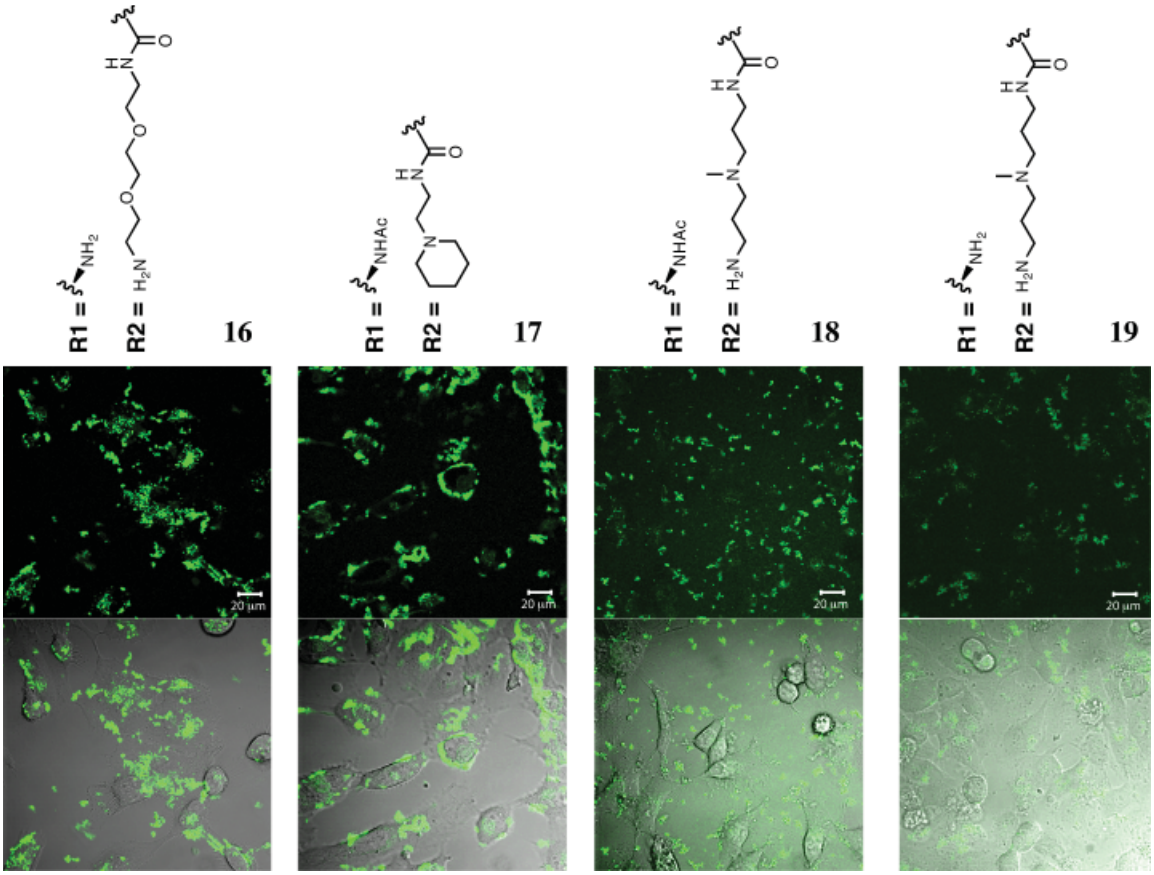

Figure E.7 Fluorescent polyamide cell uptake studies **16**-**19**. 2-Photon laser imaging setup and polyamide dosing concentration as described in Figure E.2.

of the polyamide however the polyamide appears to be localized in acidic vessicles (potentially lysosomes) as in Figures E.3–E.6. Figure E.12 also shows that treatment of the cells with ethanol allows the polyamide to readily traffic to the nucleus with significant nuclear localization after 2 h and complete localization after 4 h. Next the effect of a commonly used transfection reagent (Lipofectamine 2000) on polyamide nuclear localization was investigated (Figure E.13). The results show that the transfection reagent has little to no affect on the nuclear localization of this class of polyamide, however increased extracellular aggregation was observed.

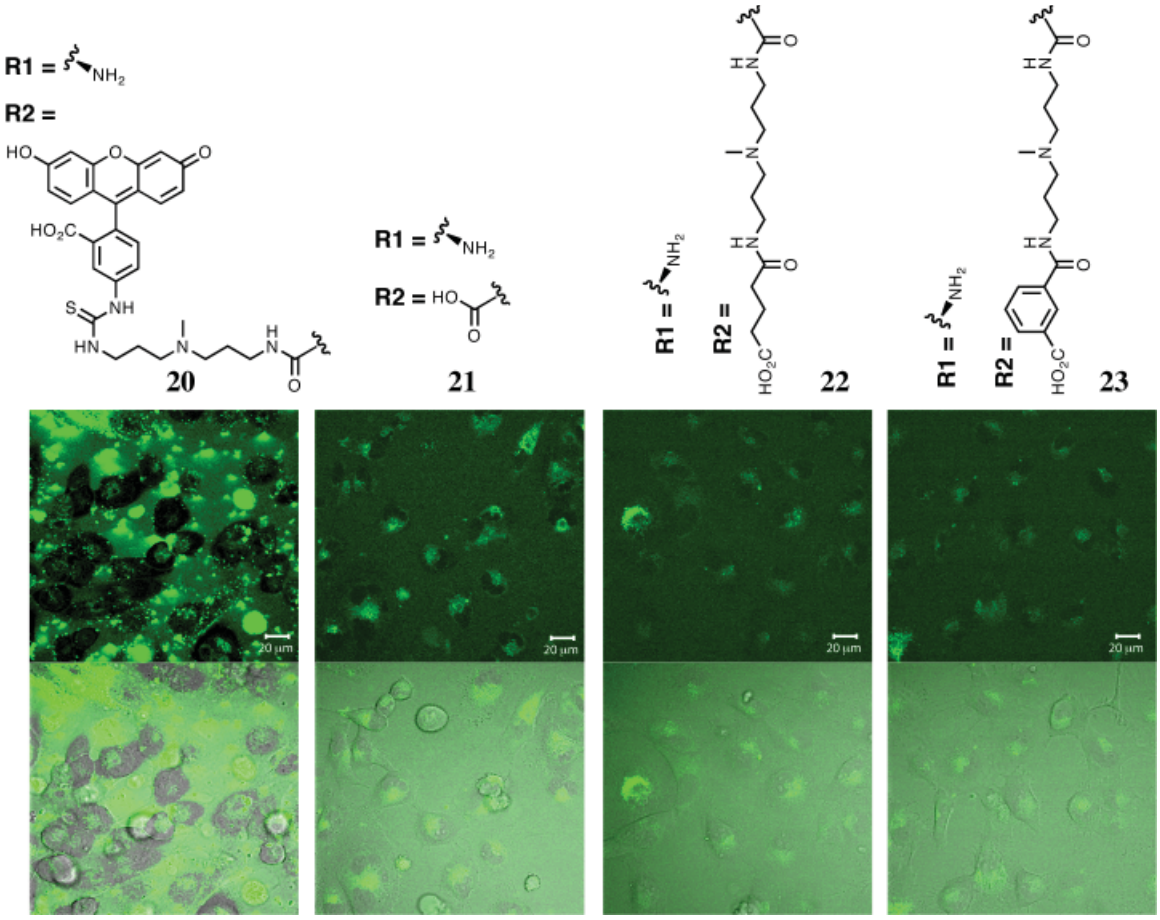

Figure E.8 Fluorescent polyamide cell uptake studies **20**–**23**. 2-Photon laser imaging setup and polyamide dosing concentration as described in Figure E.2.

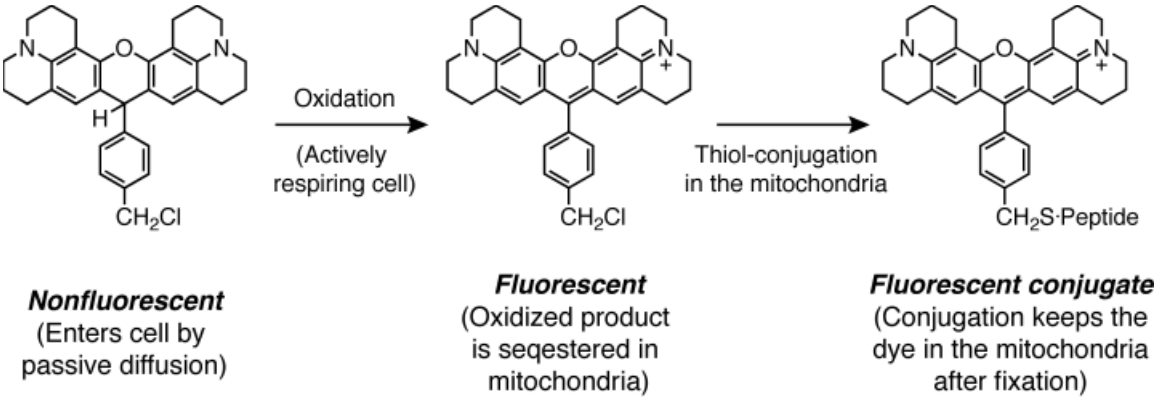

Figure E.9 Mechanism of mitochondrial staining using MitoTracker.

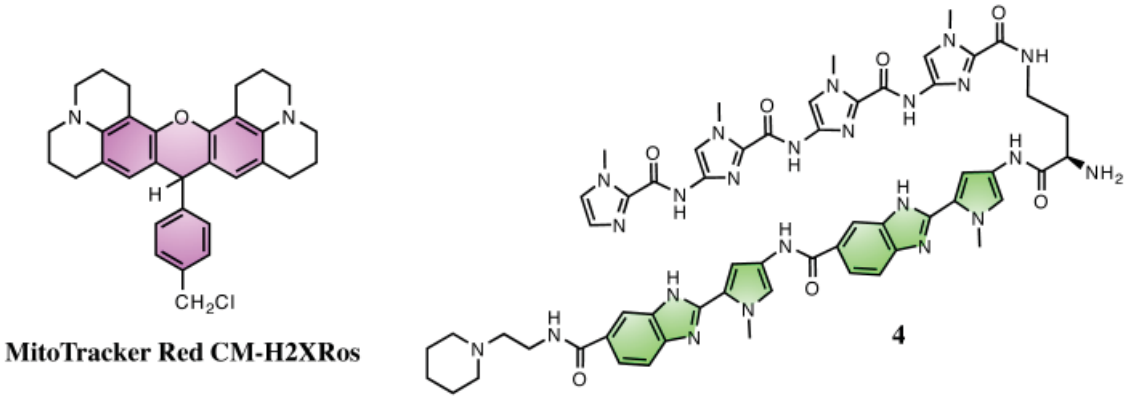

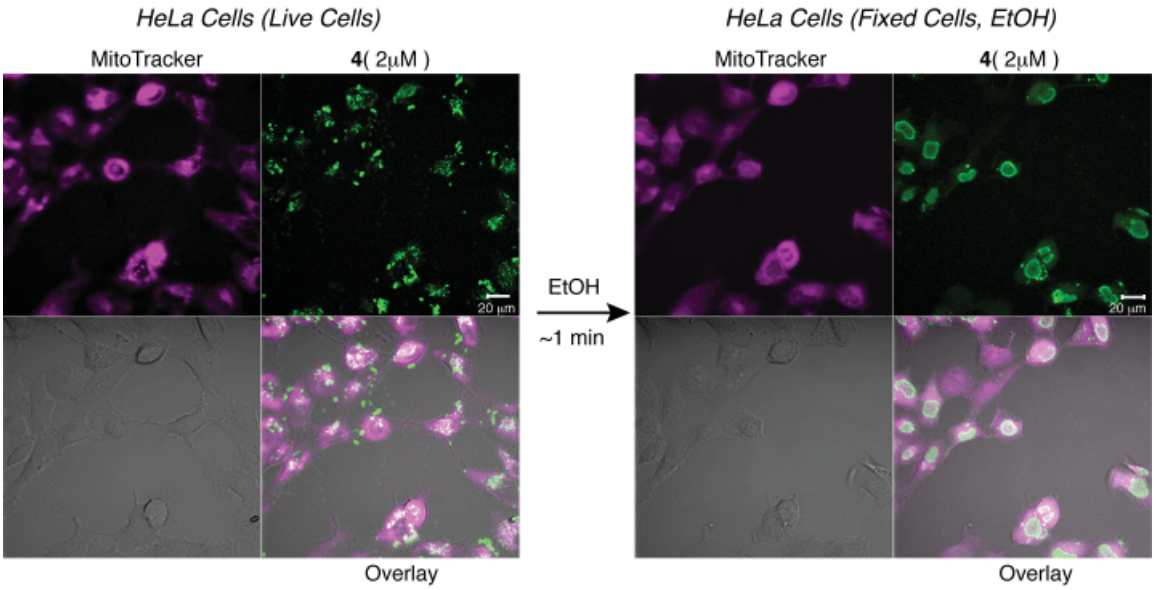

Figure E.10 Results of HeLa cell uptake study using MitoTracker and compound **4**. Dual Laser Imaging Setup: Coherent Chameleon 2-photon Laser, (λ = 810 nm, 5% power), HFT KP 680 dichroic, BP 480-520 nm MitoTracker, HeNe Laser (λ = 543 nm, 10% power), HFT KP 680 dichroic, BP 565-615 nm

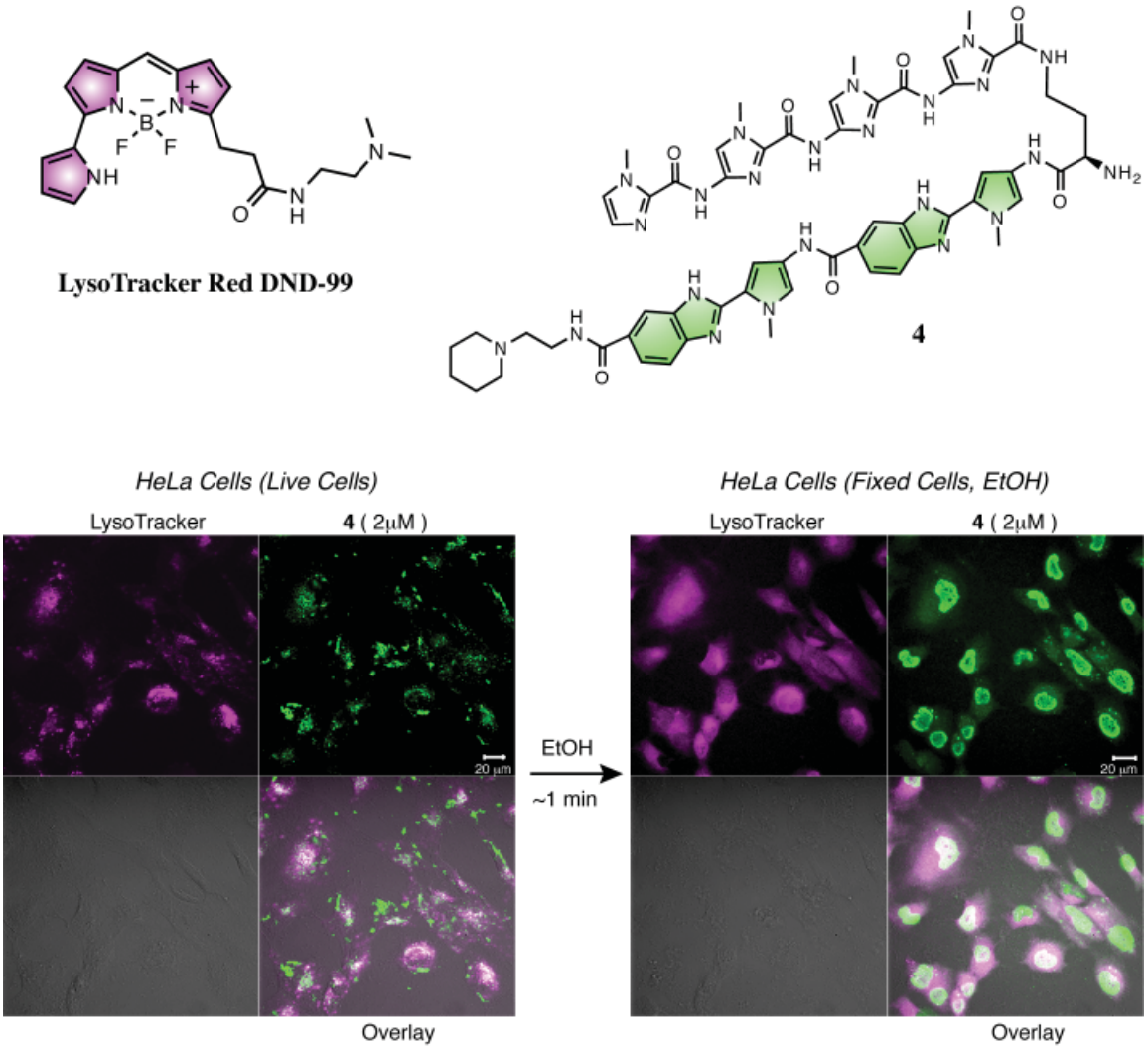

Figure E.11 Results of HeLa cell uptake study using Lysotracker and compound **4**. Dual Laser Imaging Setup: Coherent Chameleon 2-photon Laser, (λ = 810 nm, 5% power), HFT KP 680 dichroic, BP 480-520 nm LysoTracker, HeNe Laser (λ = 543 nm, 10% power), HFT KP 680 dichroic, BP 565-615 nm

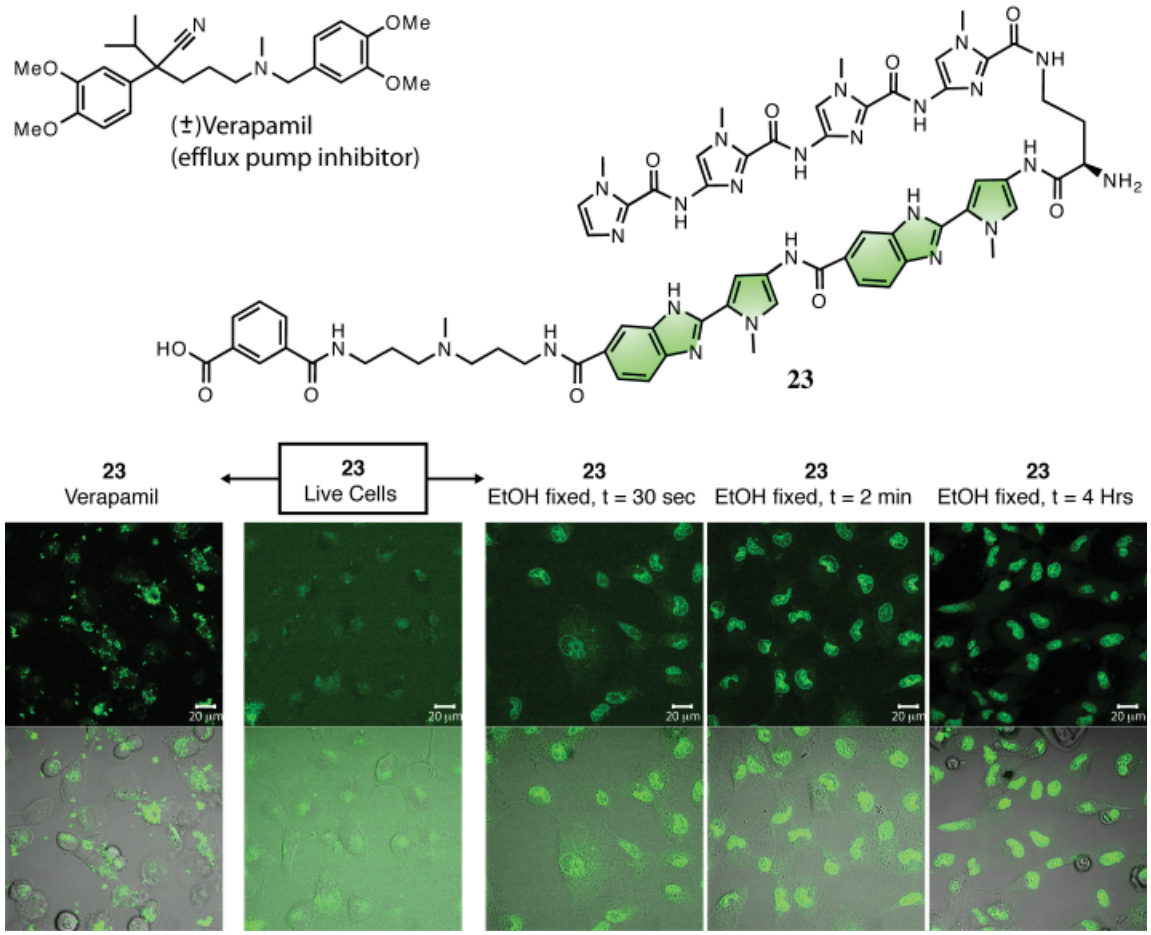

Figure E.12 Cell uptake with (±)-verapamil. Compound **23** concentration = 2μM in all experiments and (±)-verapamil concentration = 100μM. HeLa cells used in all experiments. 2-Photon Laser Imaging Setup: Coherent Chameleon 2-photon Laser, (λ = 810 nm, 5% power), HFT KP 680 dichroic, BP 480-520 nm

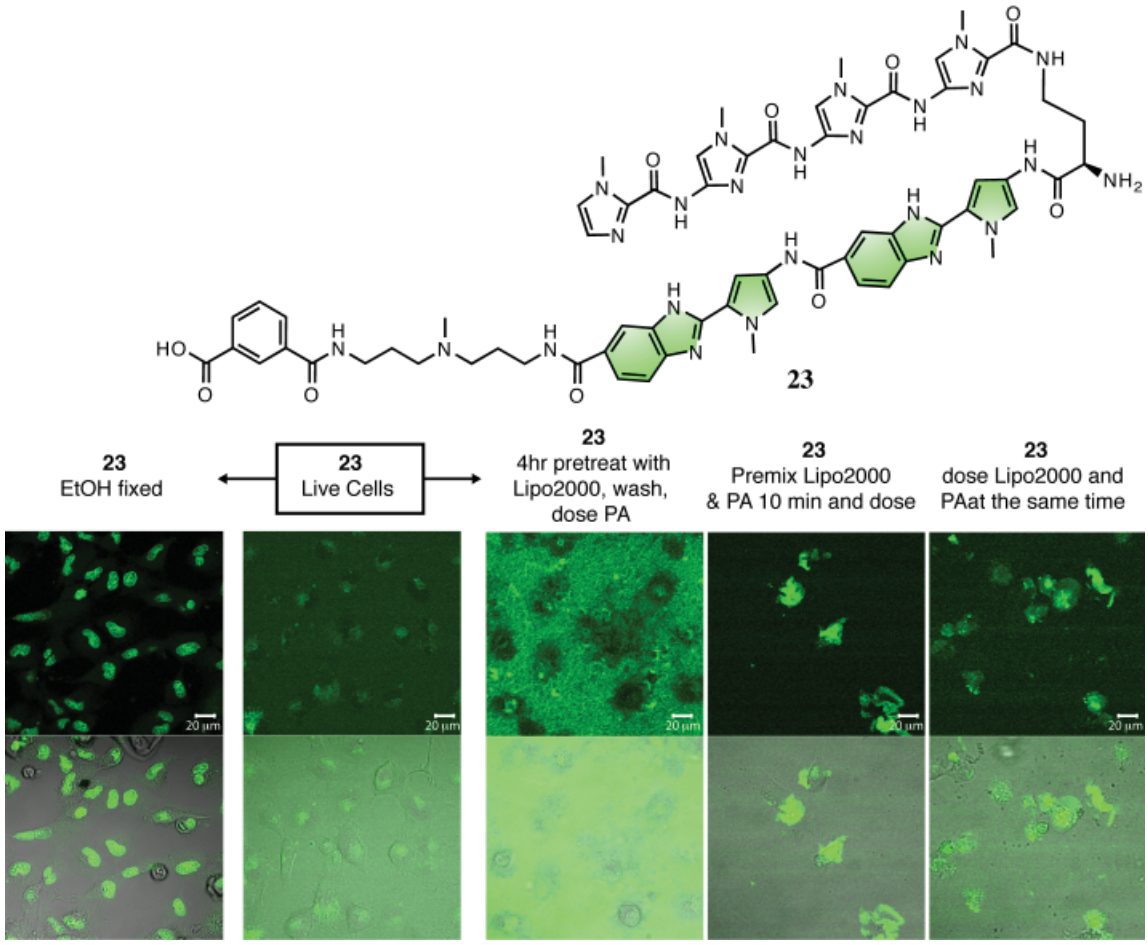

Figure E.13 Cell uptake study with Lipofectamine 2000 and compound **23** (concentration = 2μM in all experiments). Lipofectamine 2000 (Lipo2000) concentration = 1μL/150μL media. HeLa cells used in all experiments. 2-Photon Laser Imaging Setup: Coherent Chameleon 2-photon Laser, (λ = 810 nm, 5% power), HFT KP 680 dichroic, BP 480-520 nm

E.3 Conclusion

The results presented in these studies of a focused 23-member library of tail and turn modified polyamides demonstrate that the uptake properties of benzimidazole-containing polyamides, targeted to the sequence 5'-WGGGGW-3', can be divided into 2 broad categories. The first category includes compounds that are intracellular but non-nuclear, displaying a punctate cytoplasmic staining. The second category of compounds remain extracellular and have overall poor cellular uptake properties. Localization studies of non-nuclear intracellular polyamides indicated lysosomal sequestering as determined by LysoTracker Red DND-99 colocalization studies. This is in stark contrast to observations by Lown and coworkers who found that fluorescently-labeled dystamycin derivatives localized primarily to the mitochondria of human ovarian adenocarcinoma

cells (SKOV-3).[5] In addition, the mechanism of poor uptake for compound **23** was investigated using the efflux pump inhibitor (±)-verapamil[7] and results from this study indicate that inhibition of efflux pumps causes rapid cellular uptake, however lysosomal sequestration is observed as indicated by colocalization studies with LysoTracker. As documented previously, ethanol fixing of cells causes rapid nuclear uptake due to increased membrane permeability.[2-4] It has been reported that weakly basic amines selectively accumulate in cellular compartments with low internal pH and can be used to investigate the biosynthesis and pathogenesis of lysosomes.[6] In addition to the use of weakly basic amines on the tail and turns of polyamides, high imidazole content has also been shown to be a negative determinant of nuclear localization.[3,4] Currently, the cell uptake of high imidazole-containing polyamide sequences[1] remains an unsolved problem.

E.4 Experimental

Synthesis of polyamides **1**–**23** was performed according to general solid phase synthesis protocols outlined in Chapter 7 and MALDI-TOF-MS data for all compounds is presented in Section E.6. The setup for 2-photon confocal laser scanning microscopy is reported in figure captions in this appendix.

E.5 Notes and References

1. Chenoweth, D. M., Poposki, J. A., Marques, M. A., and Dervan, P. B. Programmable oligomers targeting 5'-GGGG-3' in the minor groove of DNA and NF-kappaB binding inhibition. *Bioorg. Med. Chem.* **2007,** *15*, 759–770.

2. Belitsky, J. M., Leslie, S. J., Arora, P. S., Beerman, T. A., and Dervan, P. B. Cellular uptake of *N*-methylpyrrole/*N*-methylimidazole polyamide-dye conjugates. *Bioorg. Med. Chem.* **2002,** *10*, 3313–3318.

3. Best, T. P., Edelson, B. S., Nickols, N. G., and Dervan, P. B. Nuclear localization of pyrrole-imidazole polyamide-fluorescein conjugates in cell culture. *Proc. Natl. Acad. Sci. U. S. A.* **2003,** *100*, 12063–12068.

4. Edelson, B. S., Best, T. P., Olenyuk, B., Nickols, N. G., Doss, R. M., Foister, S., Heckel, A., and Dervan, P. B. Influence of structural variation on nuclear localization of DNA-binding polyamide-fluorophore conjugates. *Nucleic. Acids. Res.* **2004,** *32*, 2802–2818.

5. Sharma, S. K., Morrissey, A. T., Miller, G. G., Gmeiner, W. H., and Lown, J. W. Design, synthesis, and intracellular localization of a fluorescently labeled DNA binding polyamide related to the antibiotic distamycin. *Bioorg. Med. Chem. Lett.* **2001,** *11*, 769–772.

6. Griffiths, G., Hoflack, B., Simons, K., Mellman, I., and Kornfeld, S. The mannose 6-phosphate receptor and the biogenesis of lysosomes. *Cell.* **1988,** *52*, 329–341.

7. Bellamy, W. T. P-glycoproteins and multidrug resistance. *Annu. Rev. Pharmacol. Toxicol.* **1996,** *36*, 161–183.

E.6 Spectra and Supplemental Information

1: MALDI-TOF-MS calculated for [M]: 1155.51, observed $[M+H]^+$: 1156.13

2: MALDI-TOF-MS calculated for [M]: 1348.63, observed $[M+H]^+$: 1348.54

3: MALDI-TOF-MS calculated for [M]: 1240.57, observed $[M+H]^+$: 1241.63

4: MALDI-TOF-MS calculated for [M]: 1181.53, observed $[M+H]^+$: 1182.50

5: MALDI-TOF-MS calculated for [M]: 1112.47, observed $[M+H]^+$: 1113.76

6: MALDI-TOF-MS calculated for [M]: 1084.44, observed $[M+H]^+$: 1085.58

7: MALDI-TOF-MS calculated for [M]: 1114.45, observed $[M+H]^+$: 1115.53

8: MALDI-TOF-MS calculated for [M]: 1128.47, observed $[M+H]^+$: 1129.78

9: MALDI-TOF-MS calculated for [M]: 1362.57, observed $[M+H]^+$: 1363.71

10: MALDI-TOF-MS calculated for [M]: 1183.51, observed $[M+H]^+$: 1184.55

11: MALDI-TOF-MS calculated for [M]: 1197.52, observed $[M+H]^+$: 1198.74

12: MALDI-TOF-MS calculated for [M]: 1197.52, observed $[M+H]^+$: 1198.45

13: MALDI-TOF-MS calculated for [M]: 1141.50, observed $[M+H]^+$: 1142.37

14: MALDI-TOF-MS calculated for [M]: 1153.50, observed $[M+H]^+$: 1154.61

15: MALDI-TOF-MS calculated for [M]: 1178.49, observed $[M+H]^+$: 1179.76

16: MALDI-TOF-MS calculated for [M]: 1201.52, observed $[M+H]^+$: 1202.90

17: MALDI-TOF-MS calculated for [M]: 1223.54, observed $[M+H]^+$: 1224.59

18: MALDI-TOF-MS calculated for [M]: 1240.57, observed $[M+H]^+$: 1241.60

19: MALDI-TOF-MS calculated for [M]: 1198.55, observed $[M+H]^+$: 1199.50

20: MALDI-TOF-MS calculated for [M]: 1587.59, observed $[M\text{-FITC}]^+$: 1199.90;
ESI-MS calculated for [M]: 1587.6, observed $[M+H]^+$: 1588.1

21: MALDI-TOF-MS calculated for [M]: 1071.41, observed $[M+H]^+$: 1072.51

22: MALDI-TOF-MS calculated for [M]: 1312.58, observed $[M+H]^+$: 1313.53

23: MALDI-TOF-MS calculated for [M]: 1346.57, observed $[M+H]^+$: 1347.78